miR-351-5p aggravates lipopolysaccharide-induced acute lung injury via inhibiting AMPK

FEN HU[1*], XIANFENG DONG[1*], WEIXIN LI[1*], JIANFA LV[2], FENG LIN[3], GAN SONG[3], GUOQIANG HOU[4] and RUIYUN LI[5]

[1]Department of Pulmonary and Critical Care Medicine, The First People's Hospital of Jiangxia District, Wuhan, Hubei 430200; [2]Department of Thoracic Surgery, Hanchuan People's Hospital, Xiaogan, Hubei 431600; [3]Department of Thoracic Surgery, Macheng People's Hospital, Huanggang, Hubei 438300; [4]Department of Thoracic Surgery, Yangxin People's Hospital, Huangshi, Hubei 435200; [5]Department of Pulmonary and Critical Care Medicine, Renmin Hospital of Wuhan University, Wuhan, Hubei 430060, P.R. China

Received December 9, 2020; Accepted April 22, 2021

DOI: 10.3892/mmr.2021.12330

Abstract. Inflammation and oxidative stress have indispensable roles in the development of acute lung injury (ALI). MicroRNA (miRNA/miR)-351-5p was initially identified as a myogenesis-associated miRNA; however, its role in lipopolysaccharide (LPS)-induced ALI remains unclear. The aim of the present study was to investigate the role and potential mechanisms of miR-351-5p in ALI. ALI was induced through a single intratracheal injection of LPS for 12 h, and miR-351-5p agomir, antagomir or their corresponding negative controls were injected into the tail vein before LPS stimulation. Compound C, 2',5'-dideoxyadenosine and H89 were used to inhibit AMP-activated protein kinase (AMPK), adenylate cyclase and protein kinase A (PKA), respectively. miR-351-5p levels in the lungs were significantly increased in response to LPS injection. miR-351-5p antagomir alleviated, while miR-351-5p agomir aggravated LPS-induced oxidative stress and inflammation in the lungs. The present results also demonstrated that miR-351-5p antagomir attenuated LPS-induced ALI via activating AMPK, and that the cAMP/PKA axis was required for the activation of AMPK by the miR-351-5p antagomir. In conclusion, the present study indicated that miR-351-5p aggravated LPS-induced ALI via inhibiting AMPK, suggesting that targeting miR-351-5p may help to develop efficient therapeutic approaches for treating ALI.

Correspondence to: Dr Ruiyun Li, Department of Pulmonary and Critical Care Medicine, Renmin Hospital of Wuhan University, 238 Jiefang Road, Wuhan, Hubei 430060, P.R. China
E-mail: 897522653@qq.com

Dr Guoqiang Hou, Department of Thoracic Surgery, Yangxin People's Hospital, 81 Ruxue Road, Huangshi, Hubei 435200, P.R. China
E-mail: 344241591@qq.com

*Contributed equally

Key words: acute lung injury, microRNA-351-5p, oxidative stress, inflammation, AMP-activated protein kinase

Introduction

Acute lung injury (ALI) is a life-threatening lung disease that can lead to refractory hypoxemia and respiratory failure. Previous studies demonstrated that the age-adjusted incidence of ALI was 86.2 per 100,000 person-years and that the in-hospital mortality rate was 38.5% (1). Sepsis is a life-threatening disease and may cause systemic inflammatory response syndrome and multiple organ dysfunction, leading to high mortality among patients in the intensive care unit (2,3). The lung is one of the most vulnerable target organs during sepsis, and septic patients often have ALI, which in turn facilitates the development of sepsis and multiple organ failure via causing gas exchange impairment and intractable hypoxemia (4-6). The pathogenesis of ALI involves the death of the pulmonary endothelium and epithelium, autophagic disorder and damage to the alveolar-capillary barrier. Thus, inflammation and oxidative stress have indispensable roles in the development of ALI (7-9). During ALI, leukocytes (e.g., macrophages and neutrophils) penetrate the lung interstitium and release substantial proinflammatory cytokines to amplify the inflammatory response. These leukocytes also increase the production of reactive oxygen species (ROS) and induce oxidative damage to lung cells. Additionally, excessive ROS levels activate NACHT, LRR and PYD domain-containing protein 3 (NLRP3) inflammasome, thereby accelerating the maturation and release of proinflammatory cytokines (10-13). Hence, it is reasonable to target inflammation and oxidative stress to develop therapeutic strategies against ALI.

AMP-activated protein kinase (AMPK) has been identified as an energy sensor in eukaryotic cells and has multiple biological functions, including anti-inflammatory and antioxidant capacities (14-17). Zhao *et al* (18) previously found that AMPK activation attenuated nuclear factor-κB (NF-κB) transcription

activity via increasing TANK-binding kinase 1 phosphorylation, thereby preventing adipose tissue inflammation. AMPK also suppressed NLRP3 inflammasome activation and alleviated lipopolysaccharide (LPS)-induced ALI in mice (7,19). Nuclear factor erythroid-2 related factor 2 (NRF2) functions as a redox-sensitive transcription factor and is required for the synthesis of various antioxidant enzymes, including superoxide dismutase (SOD), catalase (CAT) and glutathione peroxidase (GPx) (20-22). AMPK works upstream of NRF2, and AMPK-mediated NRF2 activation protects against the development of LPS-induced ALI (7,23,24). These findings distinctly define AMPK as a strategic cellular target for the treatment of ALI.

MicroRNAs (miRNA/miR) are a group of endogenous short noncoding RNAs that act as negative gene regulators via directly binding to the 3'-untranslated regions (UTRs) of downstream messenger RNAs (25-27). Numerous miRNAs have been proven to be essential for the pathogenesis of ALI (28). miR-351-5p was initially identified as a myogenesis-associated miRNA and is responsible for skeletal muscle development by targeting the phosphorylation kinase signaling cascade (29). Previous results demonstrated that an miR-351-5p agomir increased inflammation, oxidative stress and apoptosis, thereby aggravating intestinal ischemia/reperfusion injury, whereas inhibiting miR-351-5p, either by antagomir or dioscin, markedly ameliorated intestinal ischemia/reperfusion injury in mice (30-32). In addition, da Silva *et al* (33) determined that miR-351-5p repressed PTEN expression and was essential for establishing a proinflammatory environment in the H9c2 cell line. The aim of the present study was to investigate the role and potential mechanisms of miR-351-5p in ALI.

Materials and methods

Reagents and antibodies. LPS (from *Escherichia coli* O111:B4; cat. no. L2360), H89 [a specific protein kinase A (PKA inhibitor); cat. no. B1427] and the selective adenylate cyclase (AC) inhibitor 2',5'-dideoxyadenosine (DDA; cat. no. D7408) were purchased from Sigma-Aldrich (Merck KGaA). A lactate dehydrogenase (LDH) assay kit (cat. no. ab102526), myeloperoxidase (MPO) ELISA kit (cat. no. ab155458), malondialdehyde (MDA) assay kit (cat. no. ab118970), protein carbonyl content assay kit (cat. no. ab126287), total antioxidant capacity (TAOC) assay kit (cat. no. ab65329), total SOD activity assay kit (cat. no. ab65354), CAT activity assay kit (cat. no. ab83464), GPx assay kit (cat. no. ab102530), reduced glutathione (GSH) assay kit (cat. no. ab235670), tumor necrosis factor- α (TNF-α) ELISA kit (cat. no. ab208348), interleukin (IL-) 1β ELISA kit (cat. no. ab197742), IL-18 ELISA kit (cat. no. ab216165), cAMP assay kit (cat. no. ab65355) and protein kinase A (PKA) activity assay kit (cat. no. ab139435) were obtained from Abcam. Compound C (CC; cat. no. S7840), a selective AMPK inhibitor, was purchased from Selleck Chemicals. The Pierce BCA protein assay kit (cat. no. 23227) and 2',7'-dichlorofluorescin diacetate (DCFH-DA; cat. no. C2938) were purchased from Thermo Fisher Scientific, Inc. The TransAM® NRF2 kit (cat. no. 50296) was obtained from Active Motif, Inc. miR-351-5p agomir (cat. no. miR40000609-4-5), antagomir (cat. no. miR30000609-4-5) and their negative controls (NC) were synthesized by Guangzhou RiboBio Co., Ltd. For western blotting, the following primary antibodies were used at a dilution of 1:1,000: Anti-NRF2 (cat. no. ab137550; Abcam), anti-GAPDH (cat. no. ab8245; Abcam), anti-NLRP3 (cat. no. ab214185; Abcam), anti-caspase-1 p10 (cat. no. sc-56036; Santa Cruz Biotechnology, Inc.), anti-phosphorylated (p-) AMPK (cat. no. 2535; Cell Signaling Technology, Inc.) and anti-total (t-) AMPK (cat. no. 2603P; Cell Signaling Technology, Inc.).

Mice and treatments. A total of 180 male C57BL/6 mice (8-10 weeks old and 23-28 g weight) were purchased from Huafukang Bioscience Co., Ltd., and bred in a specific pathogen-free environment (25±2˚C, 50±5% humidity, 12-h light/dark cycle) with free access to food and water. LPS is the major constituent of the outer membrane of gram-negative bacteria and has emerged as a clinically relevant model for ALI. In the present study, LPS was used to establish a septic ALI model as previously described (7). ALI was induced through a single intratracheal injection of LPS (5 mg/kg) dissolved in 50 μl sterile saline for 12 h, while the control mice were treated with 50 μl sterile saline intratracheally (7). Arterial blood gas analysis, bronchoalveolar lavage fluid (BALF) analysis, pulmonary edema, respiratory function measurement and tissue injury biomarkers were detected to confirm the successful ALI model establishment. miR-351-5p agomir (20 nmol), antagomir (50 nmol) and their corresponding NCs were injected into the tail vein before LPS stimulation, as previously described (30). To inhibit AMPK, the mice were intraperitoneally injected with CC (20 mg/kg) every other day for a total of three treatments prior to miR-351-5p antagomir administration (34). The mice also received a single intraperitoneal injection of DDA (0.1 mg/kg) or H89 (2 mg/kg) at 6 h prior to miR-351-5p antagomir administration. For survival analysis, a lethal dose of LPS (25 mg/kg) was used as previously described (7). The mice were euthanized by a single intraperitoneal injection of sodium pentobarbital (200 mg/kg), and the lung, liver and brain were collected for further analyses. All experimental procedures strictly complied with the Animal Research: Reporting of *In Vivo* Experiments (ARRIVE) guidelines and were approved by the Animal Ethics Committee of Renmin Hospital of Wuhan University.

BALF collection and analysis. BALFs were collected through 3-round intratracheal injections with 1 ml pre-cooled sterile saline and then centrifuged at 4˚C for 10 min at 200 x g. The cell-free supernatants were used to measure total protein concentrations using the Pierce BCA protein assay kit, and TNF-α levels in BALFs were determined by ELISA kits. To determine leukocyte extravasation, the pelleted cells in BALFs were resuspended in sterile saline and counted with a hemocytometer and Wright-Giemsa staining.

Lung wet/dry (W/D) ratio. The fresh lungs were dissected and weighed immediately to obtain the lung wet weight after the blood was removed. Next, the lungs were placed in an oven at 80˚C for 96 h to obtain the constant lung dry weight (7). The lung W/D ratio was calculated as a measure of the degree of pulmonary edema.

Respiratory function measurement. A Buxco Resistance and Compliance system (Buxco Electronics, Inc.) was used to

monitor the respiratory data as previously described (4). The analysis focused on the tidal volume, dynamic lung compliance and respiratory rate.

Arterial blood gas analysis. To further determine respiratory function, arterial blood gas analysis was performed to evaluate pulmonary gas exchange as previously described (35). Briefly, 100 μl arterial blood samples were collected from the right common carotid artery of mice prior to euthanasia with a heparinized PE10 polyethylene catheter and then analyzed with an automatic blood gas analyzer.

Hematoxylin and eosin (H&E) staining. H&E staining was performed using the standard protocols. Briefly, the lungs were excised and fixed in 4% formaldehyde solution for 48 h, which were then embedded in paraffin and sectioned at 5 μm. The sections were dewaxed, hydrated and then incubated with hematoxylin for 10 min and eosin for 1 min at room temperature. The images were captured by light microscopy and appraised in a blinded manner.

Detection of oxidative stress. ROS levels in the lungs were detected by the DCFH-DA method (36,37). In brief, the lung homogenates were incubated with DCFH-DA (20 μmol/l) at 37˚C for 1 h in the dark and then analyzed using a microplate reader at excitation/emission wavelengths of 485/535 nm (7,38,39). The levels of MDA, protein carbonyls and GSH, and the activities of TAOC, SOD, GPx and CAT were assessed by the respective kits, following the manufacturers' instructions.

Measurements of the activities of LDH, NRF2, MPO and PKA and the levels of cAMP in the lungs. Lung homogenates were prepared in the assay buffer by a high-speed homogenizer (Wuhan Servicebio Technology Co., Ltd.) according to the respective manufacturer's instructions to determine the activities of LDH, MPO and PKA and the levels of cAMP using commercial kits. NRF2 transcription activity was detected using the TransAM® NRF2 kit, according to the manufacturer's instructions. Briefly, nuclear extracts were prepared from fresh lung tissues and incubated in plates coated with oligonucleotides containing an antioxidant responsive element. Subsequently, a primary antibody against NRF2 and a horseradish peroxidase (HRP)-conjugated secondary antibody were added. Then, the absorbance was read at 450 nm on a spectrophotometer with a reference wavelength of 655 nm.

Western blot analysis. Frozen lung tissues were homogenized by a high-speed homogenizer (Wuhan Servicebio Technology Co., Ltd.) and lysed in RIPA lysis buffer (cat. no. G2002; Wuhan Servicebio Technology Co., Ltd.), and total protein concentrations were measured using a Pierce BCA protein assay kit (40-42). Next, 20 μg total proteins were separated on a 10% SDS-PAGE gel according to standard protocols and electrotransferred to PVDF membranes. To block the non-specific binding of the primary antibodies, 5% BSA was used for 1 h at room temperature. Then, the membranes were incubated with the indicated primary antibodies at 4˚C overnight, followed by HRP-conjugated secondary antibodies at 1:5,000 dilution (cat. no. sc-2004 and sc-2005; Santa Cruz Biotechnology, Inc.) at room temperature for an additional 1 h. The protein bands were scanned with an electrochemiluminescence reagent and the relative band intensity was quantified using Image Lab Analyzer software (version 6.0; Bio-Rad Laboratories, Inc.).

Reverse transcription-quantitative polymerase chain reaction (RT-qPCR). Total RNA was extracted from the lungs using TRIzol™ reagent (Thermo Fisher Scientific, Inc.) and used for reverse transcription and cDNA synthesis (36,43-46). Next, qPCR was performed using the SYBR Premix Ex Taq kit (Takara Biotechnology Co., Ltd.) on a CFX96 real-time PCR detection system (Bio-Rad Laboratories, Inc.). The thermocycling conditions were as follows: 95˚C for 10 min, 40 cycles of 95˚C for 15 sec, 60˚C for 30 sec and 70˚C for 30 sec. Gene expression was measured by the $2^{-\Delta\Delta Cq}$ method and normalized to GAPDH (47). The primer sequences were: IL-1β, forward, 5'-CCGTGGACCTTCCAGGATGA-3' and reverse, 5'-GGGAACGTCACACACCAGCA-3'; IL-6, forward, 5'-AGTTGCCTTCTTGGGACTGA-3' and reverse, 5'-TCCACGATTTCCCAGAGAAC-3'; TNF-α, forward, 5'-AGCCCCCAGTCTGTATCCTT-3' and reverse, 5'-CTCCCTTTGCAGAACTCAGG-3'; NLRP3, forward, 5'-TACGGCCGTCTACGTCTTCT-3' and reverse, 5'-CGCAGATCACACTCCTCAAA-3'; ASC, forward, 5'-GACAGTACCAGGCAGTTCGT-3' and reverse, 5'-AGTCCTTGCAGGTCAGGTTC-3'; Pro-caspase-1, forward, 5'-CACAGCTCTGGAGATGGTGA-3' and reverse, 5'-CTTTCAAGCTTGGGCACTTC-3'; GAPDH, forward, 5'-ACTCCACTCACGGCAAATTC-3' and reverse, 5'-TCTCCATGGTGGTGAAGACA-3'.

Dual-luciferase reporter assay. The wild-type (WT) or mutant (MUT) 3'-UTR of adenylate cyclase type 6 (Adcy6) was cloned into the pGL3 luciferase reporter plasmid (Promega Corporation), which was then co-transfected with miR-351-5p agomir or agomir NC into H&EK293T cells using Lipofectamine™ 3000 (Thermo Fisher Scientific, Inc.). H&EK293T cells were purchased from the American Type Culture Collection. After 48 h, the cells were lysed and subjected to a dual-luciferase reporter assay using the Dual-Luciferase Reporter Assay System (Promega Corporation) and the data were normalized to *Renilla* luciferase activity according to the manufacturer's instructions.

Statistical analysis. All data were expressed as the mean ± SD and statistical analysis was performed using SPSS 23.0 (SPSS, Inc.). Comparisons between two groups were analyzed by two-tailed unpaired Student's t-test, and comparisons among multiple groups were analyzed by one-way ANOVA followed by Tukey's post hoc test where appropriate. Survival analysis was performed by the Kaplan-Meier method followed by a Mantel-Cox log rank test. $P<0.05$ was considered to indicate a statistically significant difference.

Results

miR-351-5p antagomir alleviates LPS-induced ALI. First, the expression levels of miR-351-5p were detected in the lungs of mice challenged with LPS for 0, 1, 2, 6 and 12 h. As presented in Fig. 1A, the miR-351-5p levels were significantly increased in

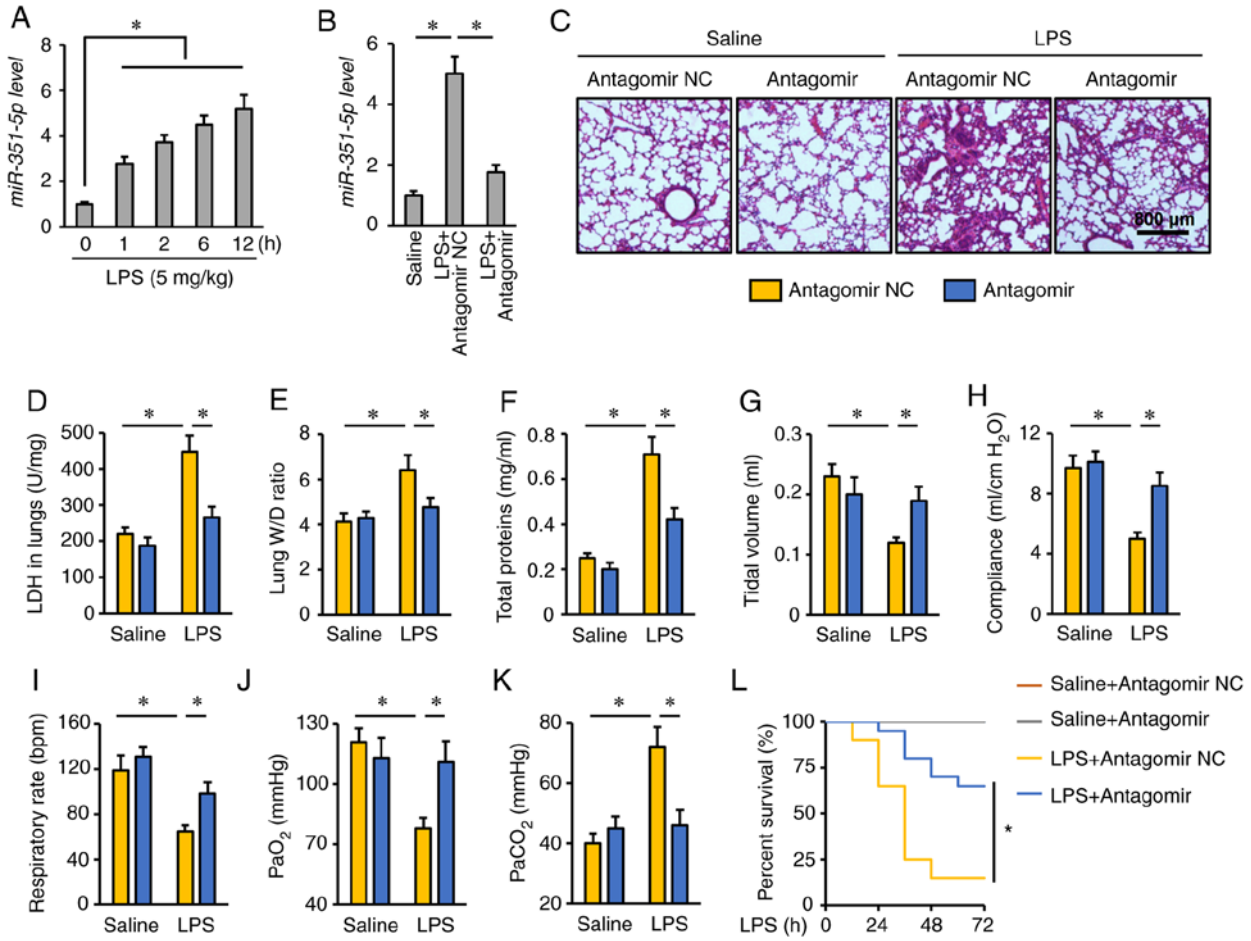

Figure 1. miR-351-5p antagomir alleviates LPS-induced ALI. (A and B) Relative miR-351-5p levels in the lungs (n=6). (C) Lung histopathology determined by hematoxylin and eosin staining (n=6). (D) LDH activity in the lungs with or without miR-351-5p antagomir treatment upon LPS challenge (n=6). (E) Lung W/D ratio (n=8). (F) Total protein concentrations in bronchoalveolar lavage fluids (n=6). (G-I) Quantification of respiratory functional parameters, including tidal volume, lung compliance and respiratory rate (n=6). (J and K) Quantification of PaO_2 and $PaCO_2$ during arterial blood gas analysis (n=6). (L) Survival analysis of mice with or without miR-351-5p antagomir treatment upon LPS challenge (n=20). All data are expressed as mean ± SD. *P<0.05 with comparisons shown by lines. miR, microRNA; LPS, lipopolysaccharide; ALI, acute lung injury; LDH, lactate dehydrogenase; W/D, wet/dry weight; PaO_2, partial pressure of oxygen; $PaCO_2$, partial pressure of carbon dioxide; NC, negative control.

response to LPS injection. To determine the role of miR-351-5p upregulation in the process of ALI, mice were treated with miR-351-5p antagomir. Tail vein injection of miR-351-5p antagomir significantly reversed the LPS-mediated upregulation of miR-351-5p in the mouse lungs (Fig. 1B). Consistent with previous reports, LPS challenge caused severe lung injury and pulmonary edema, as evidenced by H&E staining, the increased LDH activity, lung W/D ratio and total protein concentrations in BALFs, which were remarkably alleviated by the miR-351-5p antagomir (Fig. 1C-F). In addition, the mice treated with the miR-351-5p antagomir had increased tidal volume, lung compliance and respiratory rate (Fig. 1G-I). Consistently, the partial pressure of oxygen (PaO_2) was restored, while the partial pressure of carbon dioxide ($PaCO_2$) was decreased following miR-351-5p antagomir treatment (Fig. 1J and K). Notably, pretreatment with the miR-351-5p antagomir significantly improved the survival rate of LPS-challenged mice (Fig. 1L). Collectively, these data indicated that the miR-351-5p antagomir alleviated LPS-induced ALI.

miR-351-5p antagomir reduces LPS-induced oxidative stress in the lungs. Oxidative stress is a key feature in LPS-induced ALI and accelerates the progression of pulmonary injury and dysfunction (4,7). As presented in Fig. 2A, LPS induced excessive ROS generation in the lungs, and this was suppressed by the miR-351-5p antagomir. Accordingly, the levels of MDA and protein carbonyls were also decreased in mice treated with the miR-351-5p antagomir (Fig. 2B). NRF2 functions as a redox-sensitive transcription factor and is required for the synthesis of various antioxidant enzymes to scavenge excessive free radicals (20). As presented in Fig. 2C and D, NRF2 protein expression was inhibited in mice following LPS challenge but was preserved when these mice were co-treated with miR-351-5p antagomir. In addition, LPS-mediated suppression of NRF2 transcription activity in LPS-challenged lungs was reversed by the miR-351-5p antagomir (Fig. 2E). Consistently, endogenous antioxidant capacity in the lungs of mice treated with miR-351-5p antagomir was significantly increased, as evidenced by the preserved TAOC, total SOD activity, CAT activity, GPx activity and GSH levels (Fig. 2F-J). These results suggested that the miR-351-5p antagomir reduced LPS-induced oxidative stress in the lungs.

miR-351-5p antagomir inhibits LPS-induced inflammation in the lungs. Next, the present study investigated the effect

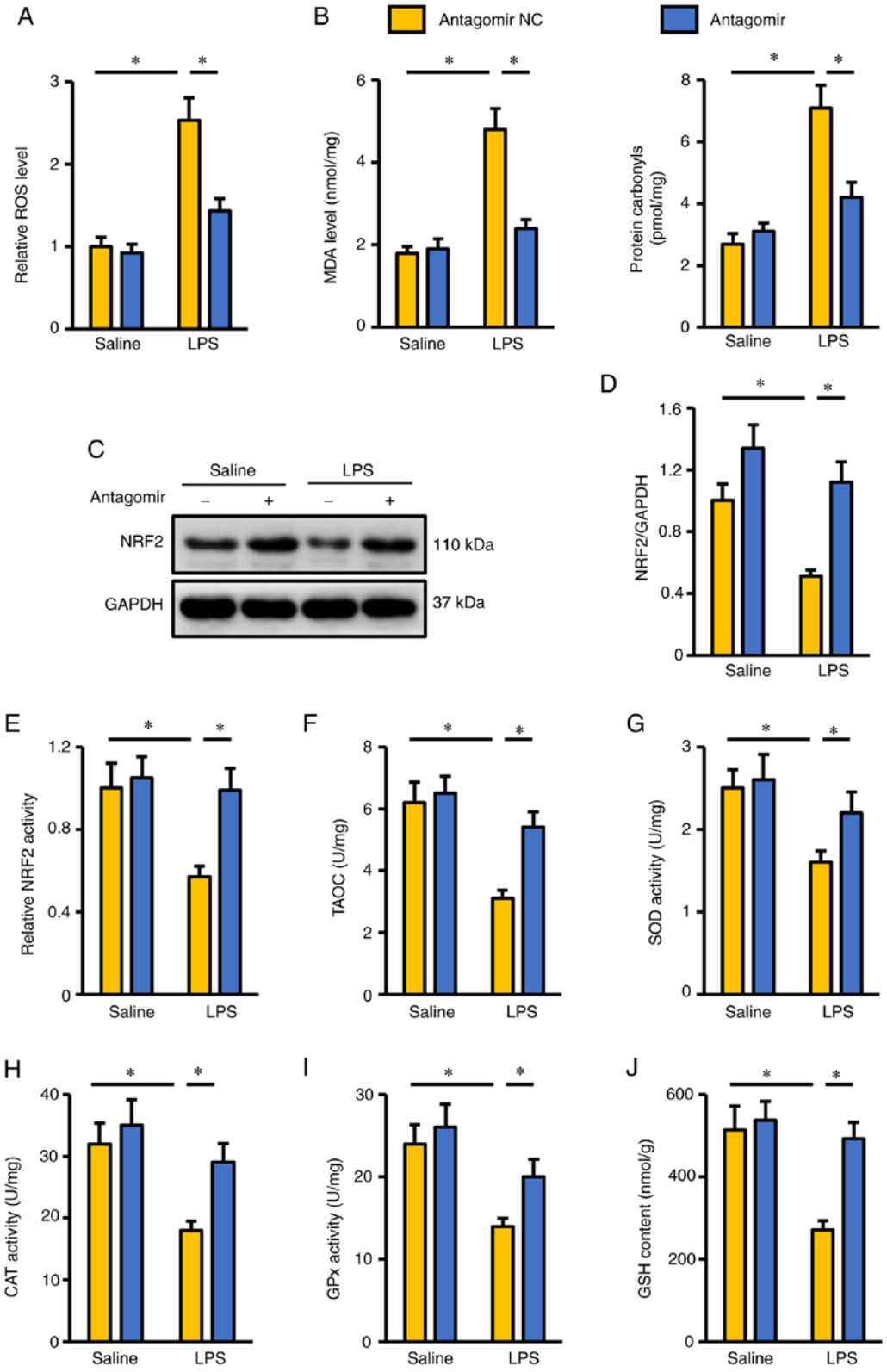

Figure 2. miR-351-5p antagomir reduces LPS-induced oxidative stress in the lungs. (A) Relative ROS levels in the lungs with or without miR-351-5p antagomir treatment upon LPS challenge (n=6). (B) MDA levels and protein carbonyls in the lungs (n=6). (C) Representative blots and (D) quantification of NRF2 protein expression levels in the lungs determined by western blot analysis (n=6). (E) Quantification of NRF2 transcription activity in the lungs (n=6). (F-J) Intracellular antioxidant capacity of the lungs determined by TAOC, total SOD activity, CAT activity, GPx activity and GSH content (n=6). All data are expressed as mean ± SD. *P<0.05 with comparisons shown by lines. miR, microRNA; LPS, lipopolysaccharide; ROS, reactive oxygen species; MDA, malondialdehyde; NRF2, nuclear factor erythroid-2 related factor 2; TAOC, total antioxidant capacity; SOD, superoxide dismutase; CAT, catalase; GPx, glutathione peroxidase; GSH, glutathione; NC, negative control.

of the miR-351-5p antagomir on LPS-induced intrapulmonary inflammatory responses in mice. The data indicated that miR-351-5p antagomir treatment effectively inhibited the mRNA expression levels of IL-1β, IL-6 and TNF-α in

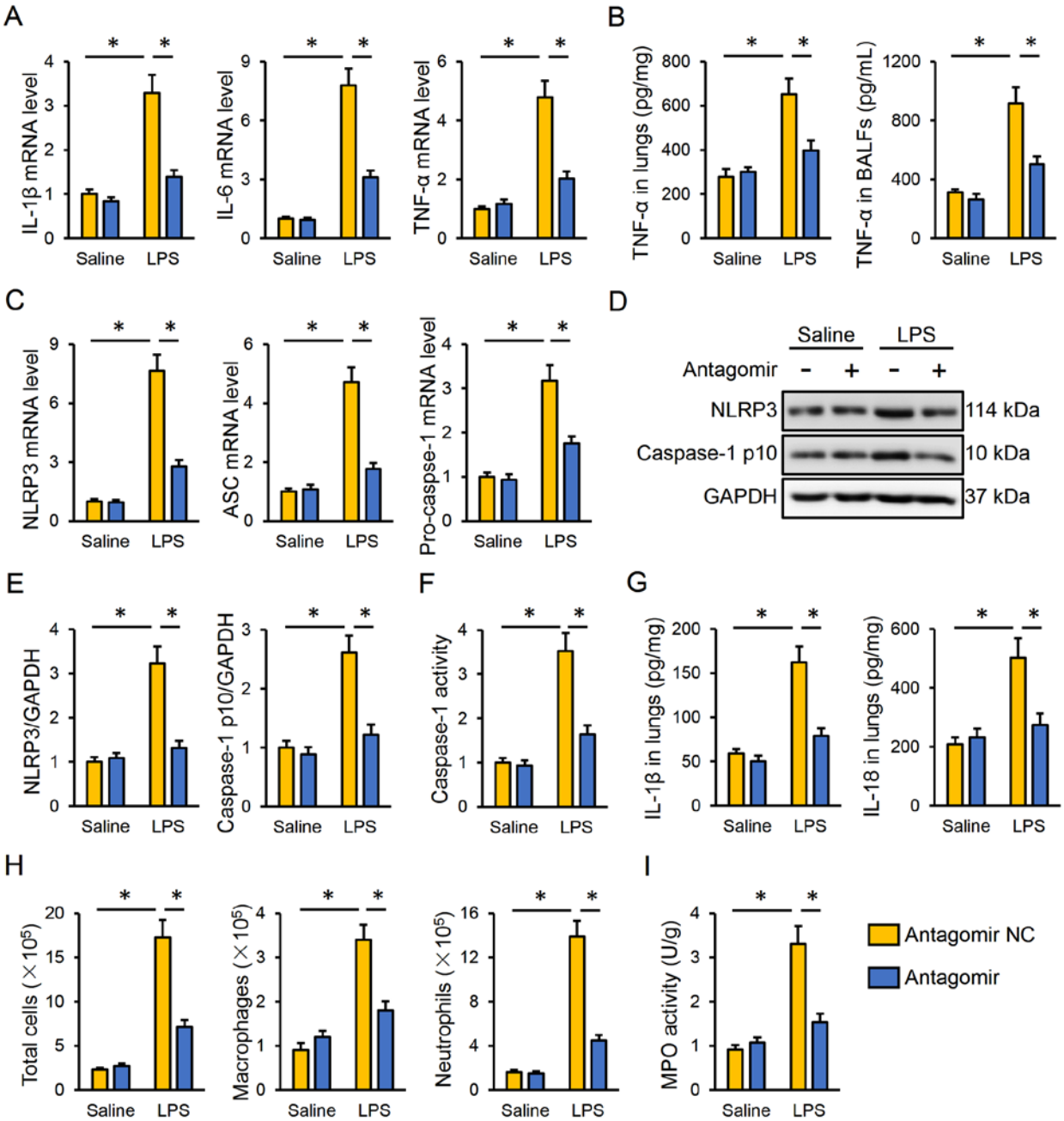

Figure 3. miR-351-5p antagomir inhibits LPS-induced inflammation and NLRP3 inflammasome in the lungs. (A) Relative mRNA expression levels of proinflammatory cytokines IL-1β, IL-6 and TNF-α in the lungs (n=6). (B) TNF-α levels in the lungs and BALFs measured by ELISA (n=6). (C) Relative mRNA expression levels of NLRP3, ASC and pro-caspase-1 in the lungs (n=6). (D) Representative blots and (E) quantification of NLRP3 and caspase-1 p10 protein expression levels determined by western blot analysis (n=6). (F) Relative caspase-1 activity (n=6). (G) IL-1β and IL-18 levels in the lungs measured by ELISA (n=6). (H) Total cells, macrophages and neutrophils in BLAFs were counted (n=6). (I) MPO activity in the lungs with or without miR-351-5p antagomir treatment upon LPS challenge (n=6). All data are expressed as mean ± SD. *P<0.05 with comparisons shown by lines. miR, microRNA; LPS, lipopolysaccharide; NLRP3, NACHT, LRR and PYD domain-containing protein 3; BALF, bronchoalveolar lavage fluid; ASC, apoptosis-associated speck-like protein containing a CARD; MPO, myeloperoxidase; NC, negative control.

the lungs (Fig. 3A). Accordingly, TNF-α protein expression levels in the lungs and BALFs were both reduced by the miR-351-5p antagomir (Fig. 3B). The NLRP3 inflammasome is a multiprotein complex responsible for the cleavage and activation of caspase-1, which subsequently promotes the maturation and release of proinflammatory cytokines, such as IL-1β and IL-18 (7,48). As presented in Fig. 3C, the miR-351-5p antagomir significantly decreased the mRNA expression levels of NLRP3, apoptosis-associated speck-like protein containing a CARD (ASC) and pro-caspase-1 in LPS-challenged lungs. The protein expression levels of NLRP3 and active caspase-1 p10 were also suppressed by the miR-351-5p antagomir in response to LPS injection (Fig. 3D and E). In addition, the miR-351-5p antagomir significantly inhibited the LPS-associated induction of caspase-1 activity (Fig. 3F). Of note, the levels of the downstream IL-1β and IL-18 were both reduced in the lungs following miR-351-5p antagomir treatment (Fig. 3G). Furthermore, pretreatment with the miR-351-5p antagomir significantly reduced the number of total cells, macrophages

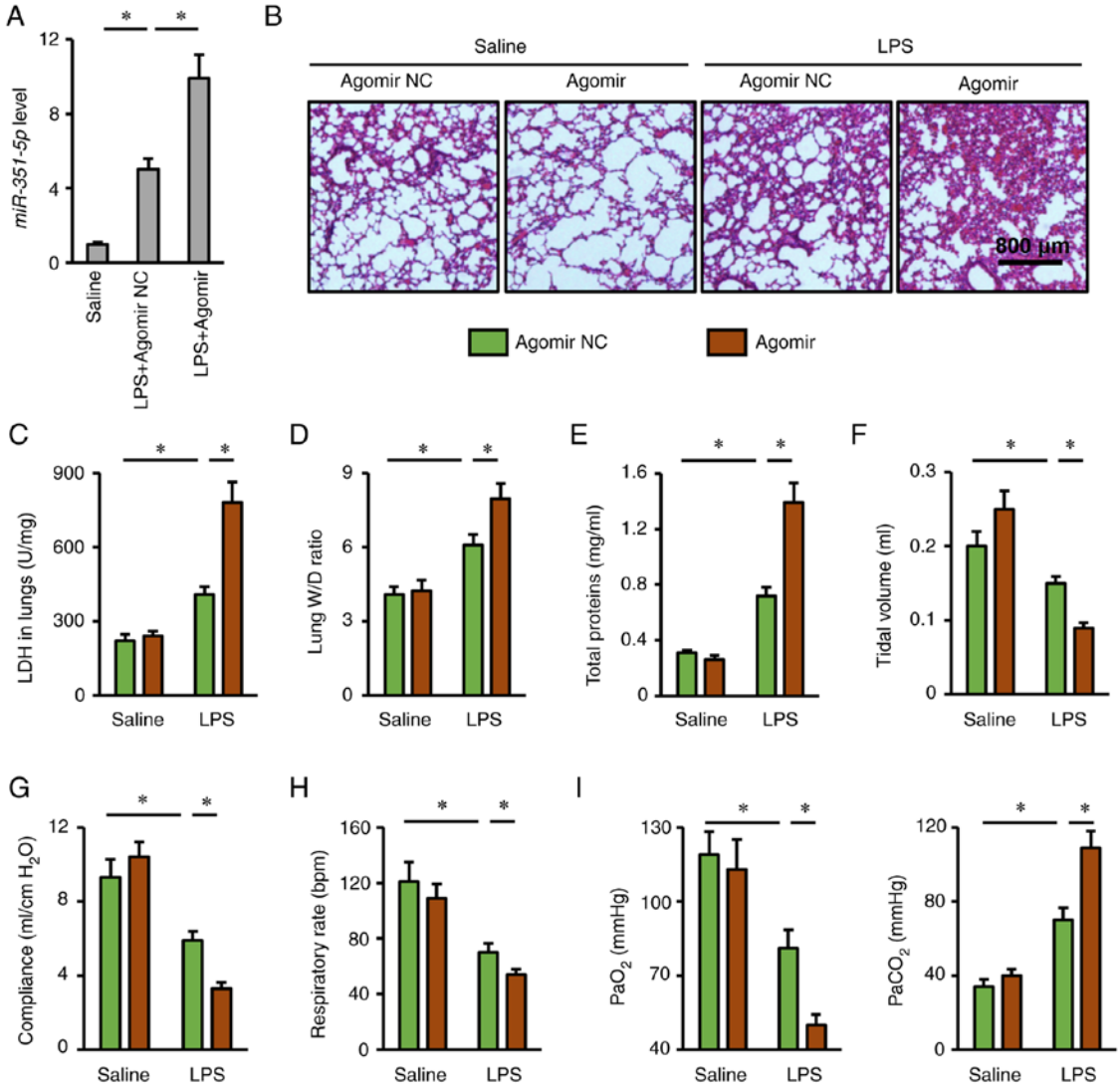

Figure 4. miR-351-5p agomir aggravates LPS-induced ALI. (A) Relative miR-351-5p expression levels in the lungs (n=6). (B) Lung histopathology determined by hematoxylin and eosin staining (n=6). (C) LDH activity in the lungs with or without miR-351-5p agomir treatment upon LPS challenge (n=6). (D) Lung W/D ratio (n=8). (E) Total prtein concentrations in bronchoalveolar lavage fluids (n=6). (F-H) Respiratory functional parameters, including tidal volume, lung compliance and respiratory rate (n=6). (I) Quantification of PaO_2 and $PaCO_2$ during arterial blood gas analysis (n=6). All data are expressed as mean ± SD. *P<0.05 with comparisons shown by lines. miR, microRNA; LPS, lipopolysaccharide; ALI, acute lung injury; LDH, lactate dehydrogenase; W/D, wet/dry weight; PaO_2, partial pressure of oxygen; $PaCO_2$, partial pressure of carbon dioxide; NC, negative control.

and neutrophils in BALFs and MPO activity in the lungs of ALI mice (Fig. 3H and I). Taken together, the present results demonstrated that the miR-351-5p antagomir inhibited LPS-induced inflammation in the lungs.

miR-351-5p agomir aggravates LPS-induced ALI. The present study also used a miR-351-5p agomir to clarify whether overexpression of miR-351-5p in the lungs could aggravate LPS-induced ALI (Fig. 4A). As expected, lung injury and pulmonary edema in mice with LPS challenge were more severe in the presence of miR-351-5p agomir, as evidenced by H&E staining, the increased LDH activity, lung W/D ratio and total protein concentrations in BALFs (Fig. 4B-E). In addition, miR-351-5p agomir treatment further reduced tidal volume, lung compliance and respiratory rate in LPS-challenged mice (Fig. 4F-H). Accordingly, LPS-associated impairment of blood gas exchange was further aggravated by the miR-351-5p agomir, as evidenced by the decreased PaO_2 and increased $PaCO_2$ (Fig. 4I). Furthermore, the survival time of miR-351-5p agomir-treated mice upon LPS challenge was no more than 24 h (data not shown). Overall, these results revealed that miR-351-5p overexpression aggravated LPS-induced ALI.

miR-351-5p agomir exacerbates LPS-induced oxidative stress and inflammation in the lungs. Next, several important biomarkers related to oxidative stress and inflammation were investigated, in order to further explore the role of miR-351-5p agomir in mice. Consistent with the ALI phenotype, the miR-351-5p agomir remarkably promoted ROS generation in LPS-challenged lungs, and the production of MDA and protein carbonyls was also increased (Fig. 5A and B). In addition, pretreatment with the miR-351-5p agomir significantly elevated TNF-α levels in the lungs and BALFs, and MPO activity in lung tissues (Fig. 5C and D). Furthermore, the numbers of total cells, macrophages and neutrophils in BALFs

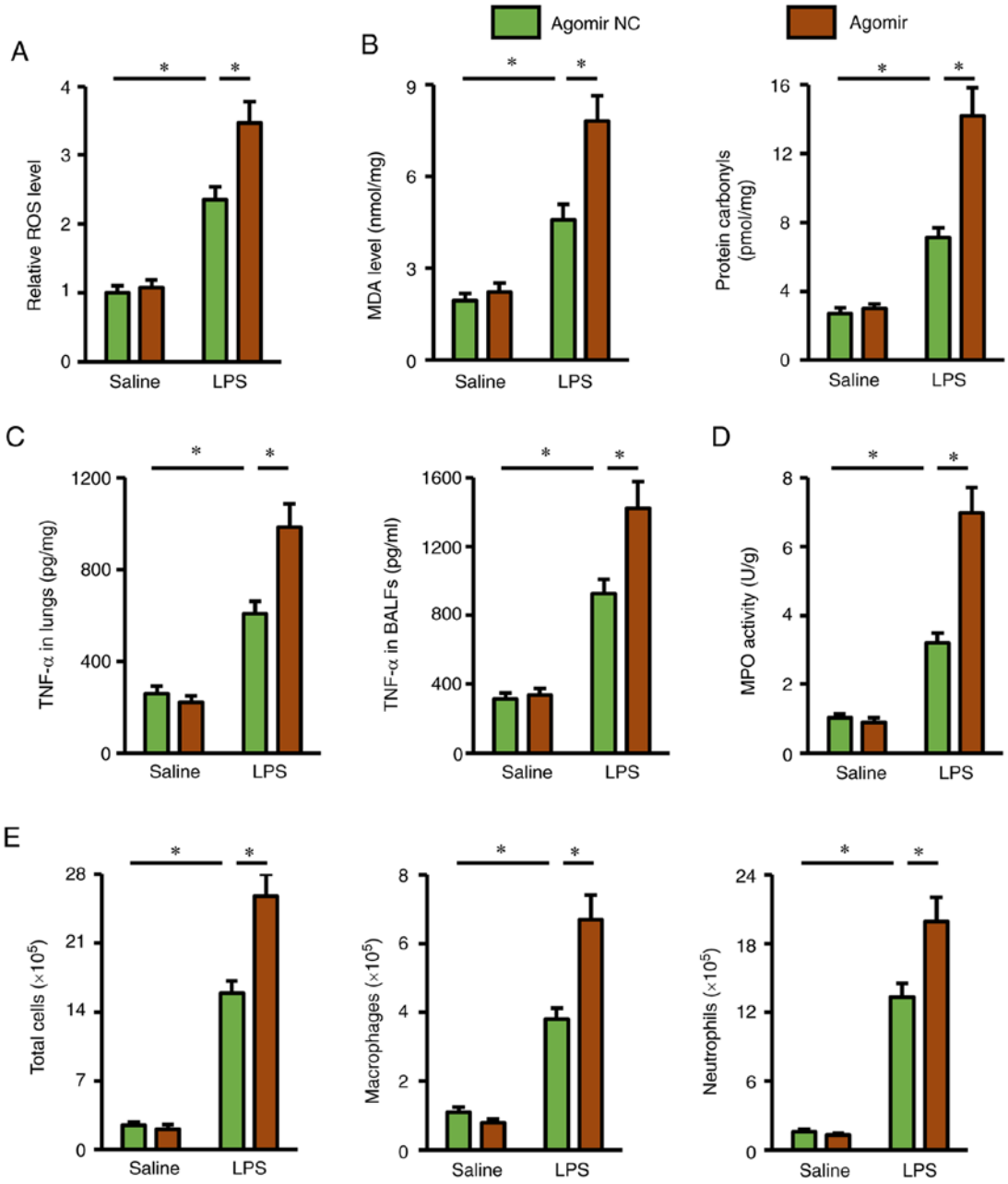

Figure 5. miR-351-5p agomir exacerbates LPS-induced oxidative stress and inflammation in the lungs. (A) Relative ROS levels in the lungs with or without miR-351-5p agomir treatment upon LPS challenge (n=6). (B) MDA level and protein carbonyls in the lungs (n=6). (C) TNF-α levels in the lungs and BALFs (n=6). (D) MPO activity in the lungs with or without miR-351-5p agomir treatment upon LPS challenge (n=6). (E) Total cells, macrophages and neutrophils in BALFs were counted (n=6). All data are expressed as mean ± SD. *P<0.05 with comparisons shown by lines. miR, microRNA; LPS, lipopolysaccharide; ROS, reactive oxygen species; MDA, malondialdehyde; BALF, bronchoalveolar lavage fluid; MPO, myeloperoxidase; NC, negative control.

from LPS-challenged mice were significantly increased by the miR-351-5p agomir (Fig. 5E). Thus, the present data demonstrated that the miR-351-5p agomir exacerbated LPS-induced oxidative stress and inflammation in the lungs.

To further confirm the therapeutic potential of miR-315-5p in mice, its effect on LPS-induced inflammation and oxidative stress in livers and brains was also evaluated. As shown in Fig. S1A, miR-315-5p antagomir-treated mice had lower intracellular ROS levels in the livers, accompanied by reduced lipid and protein peroxidation. In addition, the miR-315-5p antagomir decreased the hepatic TNF-α levels and MPO activity upon LPS stimulation (Fig. S1B and C). By contrast, the miR-315-5p agomir further aggravated LPS-induced oxidative stress and inflammation in the livers (Fig. S1D-F). Consistent with the findings in the lungs and livers, it was observed that the miR-315-5p antagomir decreased, while the miR-315-5p agomir further increased cerebral oxidative stress and inflammation upon LPS injection in mice (Fig. S2). These data further validate the therapeutic value of miR-315-5p against LPS-induced ALI.

miR-351-5p antagomir attenuates LPS-induced ALI via activating AMPK. The potential role of AMPK in the protective effects of the miR-351-5p antagomir was evaluated next. As presented in Fig. 6A and B, the miR-351-5p antagomir restored, while the miR-351-5p agomir further reduced AMPK

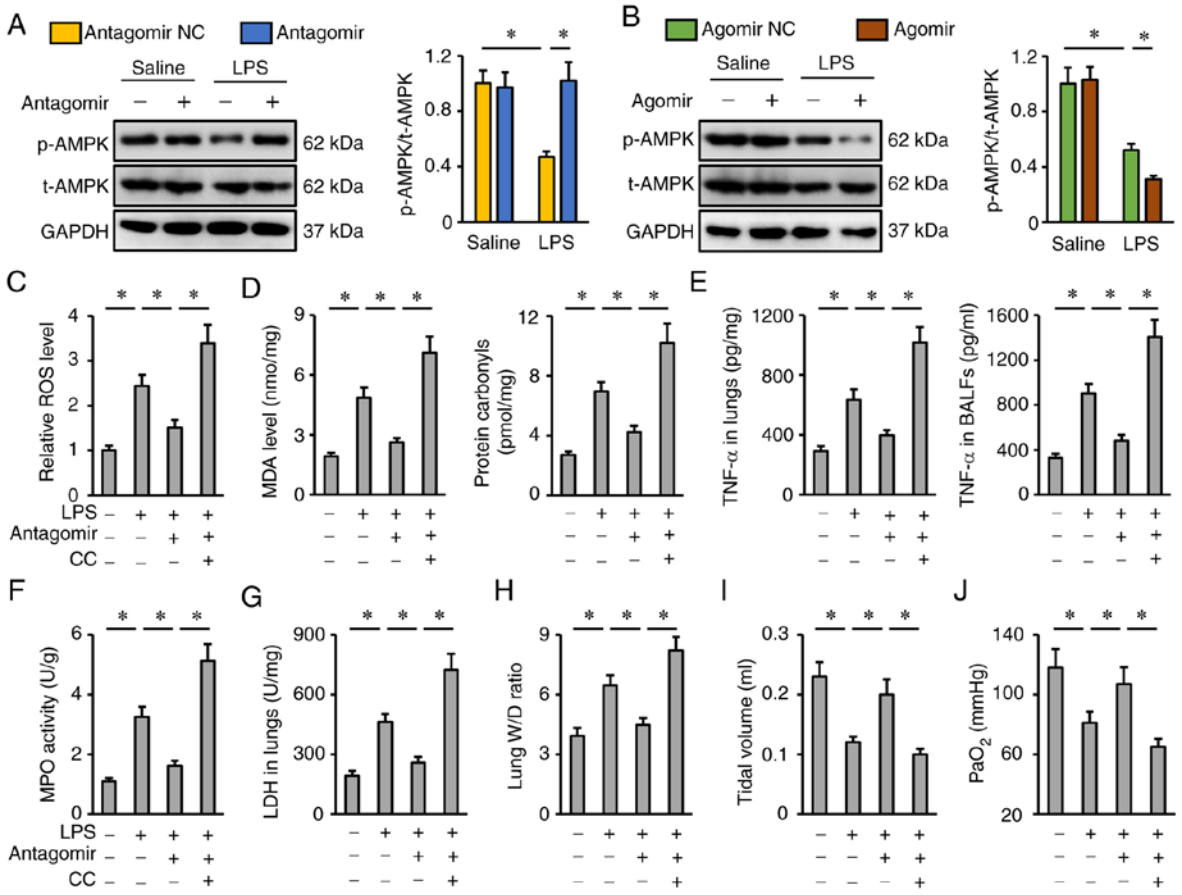

Figure 6. miR-351-5p antagomir attenuates LPS-induced ALI via activating AMPK. (A and B) Representative blots and quantification of t-AMPK and p-AMPK protein expression levels (n=6). (C) Relative ROS levels in miR-351-5p antagomir-treated lungs with or without CC administration upon LPS challenge (n=6). (D) MDA level and protein carbonyls in the lungs (n=6). (E) TNF-α levels in the lungs and BALFs measured by ELISA (n=6). (F) MPO activity in miR-351-5p antagomir-treated lungs with or without CC administration upon LPS challenge (n=6). (G) LDH activity in the lungs (n=6). (H) Lung W/D ratio (n=8). (I) Tidal volume in miR-351-5p antagomir-treated mice with or without CC administration upon LPS challenge (n=6). (J) Quantification of PaO_2 during arterial blood gas analysis (n=6). All data are expressed as mean ± SD. *P<0.05 with comparisons shown by lines. miR, microRNA; LPS, lipopolysaccharide; ALI, acute lung injury; AMPK, AMP-activated protein kinase; t-, total; p-, phosphorylated; ROS, reactive oxygen species; CC, compound C; MDA, malondialdehyde; BALF, bronchoalveolar lavage fluid; MPO, myeloperoxidase; LDH, lactate dehydrogenase; W/D, wet/dry weight; PaO_2, partial pressure of oxygen; NC, negative control.

phosphorylation in LPS-treated lungs. To inhibit AMPK, the specific inhibitor CC was used as previously described (34). CC treatment completely abrogated the inhibitory effects of the miR-351-5p antagomir on oxidative stress and inflammation, as evidenced by the increased ROS, MDA, protein carbonyls, TNF-α levels and MPO activity in the lungs and BALFs (Fig. 6C-F). Accordingly, the reductions of the lung LDH activity and W/D ratio in miR-351-5p antagomir-treated mice upon LPS challenge were blocked by CC (Fig. 6G and H). Of note, the miR-351-5p antagomir significantly restored tidal volume and PaO_2 in LPS-treated mice, but not in those pretreated with CC (Fig. 6I-J). Collectively, it can be deduced that the miR-351-5p antagomir attenuated LPS-induced ALI via activating AMPK.

miR-351-5p antagomir activates AMPK via the cAMP/PKA axis. Finally, the present study investigated the potential molecular basis by which the miR-351-5p antagomir may activate AMPK. Using the TargetScan database, it was found that miR-351-5p might directly bind to the 3'-UTR of three isoforms of AC (AC1, AC5 and AC6), which catalyze the conversion of ATP to cAMP, and induce a rapid elevation of the levels of intracellular cAMP and the activities of PKA, the upstream activator of the AMPK pathway (Fig. 7A) (49). To validate the putative interaction between miR-351-5p and AC, a dual-luciferase reporter assay was performed. AC6 (encoded by the Adcy6 gene) functions as an important AC in the development of multiple lung disease; therefore, the WT and MUT 3'-UTR of Adcy6 were cloned to perform dual-luciferase reporter assays (50,51). As shown in Fig. 7B, the miR-315-5p agomir significantly inhibited luciferase activity in cells transfected with the WT 3'-UTR of Adcy6 but failed to inhibit luciferase activity in cells transfected with the MUT 3'-UTR. As expected, it was found that the miR-351-5p antagomir increased, while the miR-351-5p agomir decreased cAMP levels and PKA activities in LPS-treated lungs (Fig. 7C and D). Accordingly, AMPK activation by the miR-351-5p antagomir was blocked after the inhibition of AC by DDA or the inhibition of PKA by H89 (Fig. 7E). The miR-351-5p antagomir also lost its inhibitory effects on LPS-induced pulmonary oxidative damage and inflammation in the presence of DDA or H89 treatment (Fig. 7F-H). In addition, the reductions of lung LDH activity and W/D ratio in miR-351-5p antagomir-treated mice upon LPS challenge were blocked by DDA or H89 (Fig. 7I and J). Accordingly, DDA or H89 also blocked the restoration of tidal volume and PaO_2 by the miR-351-5p antagomir in LPS-treated mice (Fig. 7K and L). Taken together,

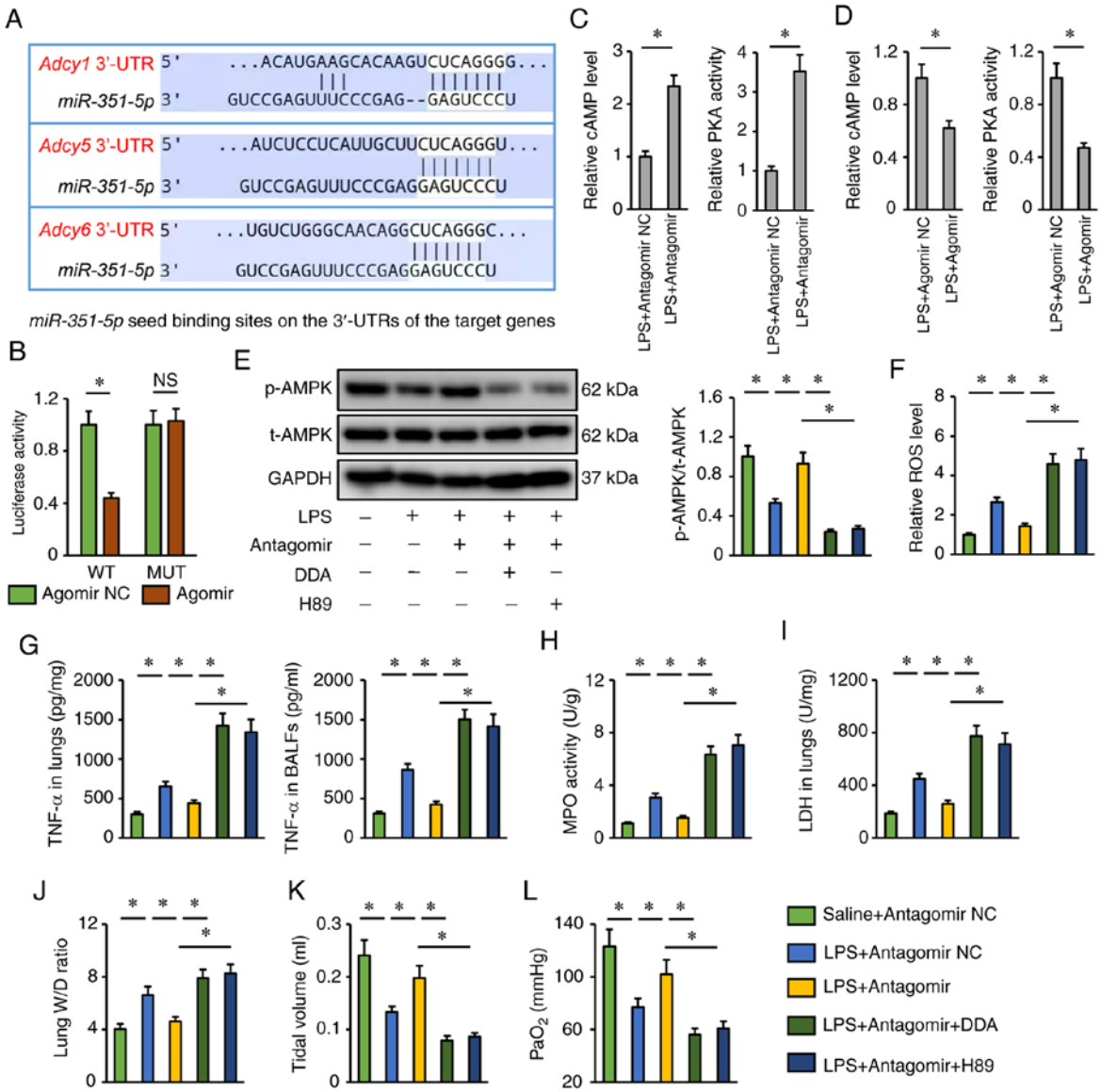

Figure 7. miR-351-5p antagomir activates AMPK via the cAMP/PKA axis. (A) Putative miR-351-5p seed binding sites on the 3'-UTRs of the target genes. (B) Relative luciferase activity in miR-351-5p antagomir-treated cells following transfection with a WT or MUT Adcy6 3'-UTR reporter (n=6). (C and D) Relative cAMP levels and PKA activities in LPS-challenged lungs with miR-351-5p antagomir or agomir treatment (n=6). (E) Western blot analysis of t-AMPK and p-AMPK protein expression levels (n=6). (F) Relative ROS levels in miR-351-5p antagomir-treated lungs with DDA or H89 administration upon LPS challenge (n=6). (G) TNF-α levels in the lungs and BALFs measured by ELISA (n=6). (H) MPO activity in miR-351-5p antagomir-treated lungs with DDA or H89 administration upon LPS challenge (n=6). (I) LDH activity in the lungs (n=6). (J) Lung W/D ratio (n=8). (K) Tidal volume in miR-351-5p antagomir-treated mice with DDA or H89 administration upon LPS challenge (n=6). (L) Quantification of PaO_2 during arterial blood gas analysis (n=6). All data are expressed as mean ± SD. *P<0.05 with comparisons shown by lines. miR, microRNA; AMPK, AMP-activated protein kinase; PKA, protein kinase A; UTR, untranslated region; WT, wild-type; MUT, mutant; LPS, lipopolysaccharide; t-, total; p-, phosphorylated; ROS, reactive oxygen species; DDA, 2',5'-dideoxyadenosine; BALF, bronchoalveolar lavage fluid; MPO, myeloperoxidase; LDH, lactate dehydrogenase; W/D, wet/dry weight; PaO_2, partial pressure of oxygen; NC, negative control; NS, not significant.

it can be concluded that the miR-351-5p antagomir activated AMPK via the cAMP/PKA axis.

Discussion

In the present study, LPS challenge was found to upregulate miR-351-5p expression in the lungs, which then directly targeted AC to decrease the intracellular cAMP levels and PKA activities, ultimately resulting in AMPK suppression and ALI progression. By contrast, miR-351-5p antagomir treatment restored AMPK phosphorylation, and significantly reduced oxidative stress and inflammation in LPS-treated mice. Overall, the present study for the first time demonstrated the involvement of miR-351-5p in the development of ALI and identified it as a promising therapeutic candidate to treat ALI.

Oxidative stress is a major pathogenic factor during ALI and directly induces oxidative damage to proteins, lipids and nucleic acids, which ultimately causes cellular dysfunction and even cell death (4,7). NRF2 functions as a signaling hub in the regulation of redox homeostasis and is essential for the transcription of multiple antioxidant enzymes (20). Upon LPS stimulation, the NRF2 protein levels are reduced, and the expression of downstream antioxidant enzymes is suppressed, resulting in a deficiency in scavenging excessive free radicals. Consistently, the present study found that the intracellular antioxidant capacity was inhibited in the lungs of mice injected with LPS, but partially preserved

in those pretreated with the miR-351-5p antagomir. Extensive inflammation also contributes to the initiation and progression of LPS-induced ALI. LPS is an exogenous ligand of Toll-like receptors and can promote NF-κB nuclear translocation to induce the transcription of various proinflammatory cytokines (35,52). In addition, LPS-associated ROS generation increases the binding of thioredoxin-interacting protein to NLRP3, which subsequently activates the NLRP3 inflammasome to accelerate the maturation and release of proinflammatory cytokines (7). The present findings demonstrated that the miR-351-5p antagomir decreased, while the miR-351-5p agomir increased NLRP3 inflammasome activation. Based on these data, it can be speculated that miR-351-5p may serve as a therapeutic target to treat ALI. However, the exact cell populations mediating the effects of miR-351-5p/AMPK during LPS-induced ALI remain unclear and need further investigation.

AMPK is a multifunctional kinase with anti-inflammatory and antioxidant capacities that has already been identified as a strategic cellular target to treat ALI (7,17,19). AC works downstream of G protein-coupled receptors and is essential for the rapid induction of intracellular cAMP synthesis, which ultimately causes PKA activation (53). PKA then phosphorylates and activates AMPK (54). miRNAs are a group of intracellular genetic regulators that also participate in regulating ALI progression. The present study found that miR-351-5p directly targeted AC and functioned as an endogenous inhibitor of the AMPK pathway. miR-351-5p antagomir treatment significantly restored intracellular cAMP levels and PKA activities, and subsequently activated AMPK to inhibit LPS-induced oxidative stress, inflammation and pulmonary dysfunction in ALI mice.

Taken together, the present results demonstrated that miR-351-5p aggravated LPS-induced ALI via inhibiting AMPK and that targeting miR-351-5p may facilitate the development of efficient therapeutic approaches for treating ALI.

Acknowledgements

Not applicable.

Funding

No funding was received.

Availability of data and materials

All data generated or analyzed during this study are included in this published article.

Authors' contributions

FH, XFD, WXL and RYL designed the experiments; FH, XFD, WXL, JFL and FL performed the experiments; JFL, FL, GS and GQH analyzed the experimental results and interpreted the data; FH, XFD and RYL wrote and revised the manuscript.All authors read and approved the final manuscript.

Ethics approval and consent to participate

All experimental procedures involving animals were approved by the Animal Ethics Committee of Renmin Hospital of Wuhan University.

Patient consent for publication

Not applicable.

Competing interests

The authors declare that they have no competing interests.

References

1. Rubenfeld GD, Caldwell E, Peabody E, Weaver J, Martin DP, Neff M, Stern EJ and Hudson LD: Incidence and outcomes of acute lung injury. N Engl J Med 353: 1685-1693, 2005.
2. Liu X, Zheng X, Wang J, Zhang N, Leung KS, Ye X and Cheng L: A long non-coding RNA signature for diagnostic prediction of sepsis upon ICU admission. Clin Transl Med 10: e123, 2020.
3. Chen H, Li Y, Wu J, Li G, Tao X, Lai K, Yuan Y, Zhang X, Zou Z and Xu Y: RIPK3 collaborates with GSDMD to drive tissue injury in lethal polymicrobial sepsis. Cell Death Differ 27: 2568-2585, 2020.
4. Yang HH, Duan JX, Liu SK, Xiong JB, Guan XX, Zhong WJ, Sun CC, Zhang CY, Luo XQ, Zhang YF, *et al*: A COX-2/sEH dual inhibitor PTUPB alleviates lipopolysaccharide-induced acute lung injury in mice by inhibiting NLRP3 inflammasome activation. Theranostics 10: 4749-4761, 2020.
5. Shah TG, Predescu D and Predescu S: Mesenchymal stem cells-derived extracellular vesicles in acute respiratory distress syndrome: A review of current literature and potential future treatment options. Clin Transl Med 8: 25, 2019.
6. Jiang J, Huang K, Xu S, Garcia J, Wang C and Cai H: Targeting NOX4 alleviates sepsis-induced acute lung injury via attenuation of redox-sensitive activation of CaMKII/ERK1/2/MLCK and endothelial cell barrier dysfunction. Redox 36: 101638, 2020.
7. Huang XT, Liu W, Zhou Y, Sun M, Yang HH, Zhang CY and Tang SY: Galectin-1 ameliorates lipopolysaccharide-induced acute lung injury via AMPK-Nrf2 pathway in mice. Free Radic Biol Med 146: 222-233, 2020.
8. Aggarwal S, Lazrak A, Ahmad I, Yu Z, Bryant A, Mobley JA, Ford DA and Matalon S: Reactive species generated by heme impair alveolar epithelial sodium channel function in acute respiratory distress syndrome. Redox Biol 36: 101592, 2020.
9. Li Y, Cao Y, Xiao J, Shang J, Tan Q, Ping F, Huang W, Wu F, Zhang H and Zhang X: Inhibitor of apoptosis-stimulating protein of p53 inhibits ferroptosis and alleviates intestinal ischemia/reperfusion-induced acute lung injury. Cell Death Differ 27: 2635-2650, 2020.
10. Jia Y, Cui R, Wang C, Feng Y, Li Z, Tong Y, Qu K, Liu C and Zhang J: Metformin protects against intestinal ischemia-reperfusion injury and cell pyroptosis via TXNIP-NLRP3-GSDMD pathway. Redox Biol 32: 101534, 2020.
11. Dai Y, Zhang J, Xiang J, Li Y, Wu D and Xu J: Calcitriol inhibits ROS-NLRP3-IL-1beta signaling axis via activation of Nrf2-antioxidant signaling in hyperosmotic stress stimulated human corneal epithelial cells. Redox Biol 21: 101093, 2019.
12. Wang Z, Xu G, Gao Y, Zhan X, Qin N, Fu S, Li R, Niu M, Wang J, Liu Y, *et al*: Cardamonin from a medicinal herb protects against LPS-induced septic shock by suppressing NLRP3 inflammasome. Acta Pharm Sin B 9: 734-744, 2019.
13. Zhou X, Wu Y, Ye L, Wang Y, Zhang K, Wang L, Huang Y, Wang L, Xian S, Zhang Y and Chen Y: Aspirin alleviates endothelial gap junction dysfunction through inhibition of NLRP3 inflammasome activation in LPS-induced vascular injury. Acta Pharm Sin B 9: 711-723, 2019.
14. Zhang X, Ma ZG, Yuan YP, Xu SC, Wei WY, Song P, Kong CY, Deng W and Tang QZ: Rosmarinic acid attenuates cardiac fibrosis following long-term pressure overload via AMPKα/smad3 signaling. Cell Death Dis 9: 102, 2018.
15. Qi G, Zhou Y, Zhang X, Yu J, Li X, Cao X, Wu C and Guo P: Cordycepin promotes browning of white adipose tissue through an AMP-activated protein kinase (AMPK)-dependent pathway. Acta Pharm Sin B 9: 135-143, 2019.
16. Rodríguez C, Contreras C, Sáenz-Medina J, Muñoz M, Corbacho C, Carballido J, Garcia-Sacristán A, Hernandez M, Lopez M, Rivera L and Prieto D: Activation of the AMP-related kinase (AMPK) induces renal vasodilatation and downregulates nox-derived reactive oxygen species (ROS) generation. Redox Biol 34: 101575, 2020.

17. Hu C, Zhang X, Wei W, Zhang N, Wu H, Ma Z, Li L, Deng W and Tang Q: Matrine attenuates oxidative stress and cardiomyocyte apoptosis in doxorubicin-induced cardiotoxicity via maintaining AMPK α/UCP2 pathway. Acta Pharm Sin B 9: 690-701, 2019.
18. Zhao P, Wong KI, Sun X, Reilly SM, Uhm M, Liao Z, Skorobogatko Y and Saltiel AR: TBK1 at the crossroads of inflammation and energy homeostasis in adipose tissue. Cell 172: 731-743, 2018.
19. Jiang WL, Zhao KC, Yuan W, Zhou F, Song HY, Liu GL, Huang J, Zou JJ, Zhao B and Xie SP: MicroRNA-31-5p exacerbates lipopolysaccharide-induced acute lung injury via inactivating cab39/AMP α pathway. Oxid Med Cell Longev 2020: 8822361, 2020.
20. Warpsinski G, Smith MJ, Srivastava S, Keeley TP, Siow R, Fraser PA and Mann GE: Nrf2-regulated redox signaling in brain endothelial cells adapted to physiological oxygen levels: Consequences for sulforaphane mediated protection against hypoxia-reoxygenation. Redox Biol 37: 101708, 2020.
21. Deng S, Essandoh K, Wang X, Li Y, Huang W, Chen J, Peng J, Jiang DS, Mu X, Wang C, *et al*: Tsg101 positively regulates P62-Keap1-Nrf2 pathway to protect hearts against oxidative damage. Redox Biol 32: 101453, 2020.
22. Zhang X, Hu C, Kong CY, Song P, Wu HM, Xu SC, Yuan YP, Deng W, Ma ZG and Tang QZ: FNDC5 alleviates oxidative stress and cardiomyocyte apoptosis in doxorubicin-induced cardiotoxicity via activating AKT. Cell Death Differ 27: 540-555, 2020.
23. Yang L, Li X, Jiang A, Li X, Chang W, Chen J and Ye F: Metformin alleviates lead-induced mitochondrial fragmentation via AMPK/Nrf2 activation in SH-SY5Y cells. Redox Biol 36: 101626, 2020.
24. Matzinger M, Fischhuber K, Pölöske D, Mechtler K and Heiss EH: AMPK leads to phosphorylation of the transcription factor Nrf2, tuning transactivation of selected target genes. Redox Biol 29: 101393, 2020.
25. Carbonell T and Gomes AV: MicroRNAs in the regulation of cellular redox status and its implications in myocardial ischemia-reperfusion injury. Redox Biol 36: 101607, 2020.
26. Wang G, Yuan J, Cai X, Xu Z, Wang J, Ocansey DK, Yan Y, Qian H, Zhang X, Xu W and Mao F: HucMSC-Exosomes carrying miR-326 inhibit neddylation to relieve inflammatory bowel disease in mice. Clin Transl Med 10: e113, 2020.
27. Wang YM, Zheng YF, Yang SY, Yang ZM, Zhang LN, He YQ, Gong XH, Liu D, Finnell RH, Qiu ZL, *et al*: MicroRNA-197 controls ADAM10 expression to mediate MeCP2's role in the differentiation of neuronal progenitors. Cell Death Differ 26: 1863-1879, 2019.
28. Wei X, Yi X, Lv H, Sui X, Lu P, Li L, An Y, Yang Y, Yi H and Chen G: MicroRNA-377-3p released by mesenchymal stem cell exosomes ameliorates lipopolysaccharide-induced acute lung injury by targeting RPTOR to induce autophagy. Cell Death Dis 11: 657, 2020.
29. Xie SJ, Li JH, Chen HF, Tan YY, Liu SR, Zhang Y, Xu H, Yang JH, Liu S, Zheng LL, *et al*: Inhibition of the JNK/MAPK signaling pathway by myogenesis-associated miRNAs is required for skeletal muscle development. Cell Death Differ 25: 1581-1597, 2018.
30. Hu Y, Tao X, Han X, Xu L, Yin L, Sun H, Qi Y, Xu Y and Peng J: MicroRNA-351-5p aggravates intestinal ischaemia/reperfusion injury through the targeting of MAPK13 and sirtuin-6. Br J Pharmacol 175: 3594-3609, 2018.
31. Hu Y, Mao Z, Xu L, Yin L, Tao X, Tang Z, Qi Y, Sun P and Peng J: Protective effect of dioscin against intestinal ischemia/reperfusion injury via adjusting miR-351-5p-mediated oxidative stress. Pharmacol Res 137: 56-63, 2018.
32. Zheng L, Han X, Hu Y, Zhao X, Yin L, Xu L, Qi Y, Xu Y, Han X, Liu K and Peng J: Dioscin ameliorates intestinal ischemia/reperfusion injury via adjusting miR-351-5p/MAPK13-mediated inflammation and apoptosis. Pharmacol Res 139: 431-439, 2019.
33. da Silva W, dos Santos RA and Moraes KC: Mir-351-5p contributes to the establishment of a pro-inflammatory environment in the H9c2 cell line by repressing PTEN expression. Mol Cell Biochem 411: 363-371, 2016.
34. Ma ZG, Dai J, Zhang WB, Yuan Y, Liao HH, Zhang N, Bian ZY and Tang QZ: Protection against cardiac hypertrophy by geniposide involves the GLP-1 receptor/AMPKα signalling pathway. Br J Pharmacol 173: 1502-1516, 2016.
35. Wang Z, Yan J, Yang F, Wang D, Lu Y and Liu L: MicroRNA-326 prevents sepsis-induced acute lung injury via targeting TLR4. Free Radic Res 54: 408-418, 2020.
36. Hu C, Zhang X, Song P, Yuan YP, Kong CY, Wu HM, Xu SC, Ma ZG and Tang QZ: Meteorin-Like protein attenuates doxorubicin-induced cardiotoxicity via activating cAMP/PKA/SIRT1 pathway. Redox Biol 37: 101747, 2020.
37. Hu C, Zhang X, Zhang N, Wei WY, Li LL, Ma ZG and Tang QZ: Osteocrin attenuates inflammation, oxidative stress, apoptosis, and cardiac dysfunction in doxorubicin-induced cardiotoxicity. Clin Transl Med 10: e124, 2020.
38. Qi S, Guo L, Yan S, Lee RJ, Yu S and Chen S: Hypocrellin A-based photodynamic action induces apoptosis in A549 cells through ROS-mediated mitochondrial signaling pathway. Acta Pharm Sin B 9: 279-293, 2019.
39. Pintado-Berninches L, Fernandez-Varas B, Benitez-Buelga C, Manguan-Garcia C, Serrano-Benitez A, Iarriccio L, Carrillo J, Guenechea G, Egusquiaguirre SP, Pedraz JL, *et al*: GSE4 peptide suppresses oxidative and telomere deficiencies in ataxia telangiectasia patient cells. Cell Death Differ 26: 1998-2014, 2019.
40. Zhang X, Zhu JX, Ma ZG, Wu HM, Xu SC, Song P, Kong CY, Yuan YP, Deng W and Tang QZ: Rosmarinic acid alleviates cardiomyocyte apoptosis via cardiac fibroblast in doxorubicin-induced cardiotoxicity. Int J Biol Sci 15: 556-567, 2019.
41. Zhou F, Mei J, Han X, Li H, Yang S, Wang M, Chu L, Qiao H and Tang T: Kinsenoside attenuates osteoarthritis by repolarizing macrophages through inactivating NF-κB/MAPK signaling and protecting chondrocytes. Acta Pharm Sin B 9: 973-985, 2019.
42. Ou T, Yang W, Li W, Lu Y, Dong Z, Zhu H, Sun X, Dong Z, Weng X, Chang S, *et al*: SIRT5 deficiency enhances the proliferative and therapeutic capacities of adipose-derived mesenchymal stem cells via metabolic switching. Clin Transl Med 10: e172, 2020.
43. Zhang X, Hu C, Zhang N, Wei WY, Li LL, Wu HM, Ma ZG and Tang QZ: Matrine attenuates pathological cardiac fibrosis via RPS5/p38 in mice. Acta Pharmacol Sin 42: 573-584, 2020.
44. Yi W, Tu MJ, Liu Z, Zhang C, Batra N, Yu AX and Yu AM: Bioengineered miR-328-3p modulates GLUT1-mediated glucose uptake and metabolism to exert synergistic antiproliferative effects with chemotherapeutics. Acta Pharm Sin B 10: 159-170, 2020.
45. Wu L, Xiang S, Hu X, Mo M, Zhao C, Cai Y, Tong S, Jiang H, Chen L, Wang Z, *et al*: Prostate-specific antigen modulates the osteogenic differentiation of MSCs via the cadherin 11-akt axis. Clin Transl Med 10: 363-373, 2020.
46. Zhang X, Hu C, Yuan YP, Song P, Kong CY, Wu HM, Xu SC, Ma ZG and Tang QZ: Endothelial ERG alleviates cardiac fibrosis via blocking endothelin-1-dependent paracrine mechanism. Cell Biol Toxicol 20: doi:10.1007, 2021.
47. Livak KJ and Schmittgen TD: Analysis of relative gene expression data using real-time quantitative PCR and the 2(-Delta Delta C(T)) method. Methods 25: 402-408, 2001.
48. Wang Y, Liu X, Shi H, Yu Y, Yu Y, Li M and Chen R: NLRP3 inflammasome, an immune-inflammatory target in pathogenesis and treatment of cardiovascular diseases. Clin Transl Med 10: 91-106, 2020.
49. Agarwal V, Bell GW, Nam JW and Bartel DP: Predicting effective microRNA target sites in mammalian mRNAs. Elife 4: e05005, 2015.
50. Birrell MA, Bonvini SJ, Wortley MA, Buckley J, Yew-Booth L, Maher SA, Dale N, Dubuis ED and Belvisi MG: The role of adenylyl cyclase isoform 6 in beta-adrenoceptor signalling in murine airways. Br J Pharmacol 172: 131-141, 2015.
51. Sayner SL, Balczon R, Frank DW, Cooper DM and Stevens T: Filamin A is a phosphorylation target of membrane but not cytosolic adenylyl cyclase activity. Am J Physiol Lung Cell Mol Physiol 301: L117-L124, 2011.
52. Schappe MS, Szteyn K, Stremska ME, Mendu SK, Downs TK, Seegren PV, Mahoney MA, Dixit S, Krupa JK, Stipes EJ, *et al*: Chanzyme TRPM7 mediates the Ca^{2+} influx essential for lipopolysaccharide-induced toll-like receptor 4 endocytosis and macrophage activation. Immunity 48: 59-74, 2018.
53. Tang T, Hammond HK, Firth A, Yang Y, Gao MH, Yuan JX and Lai NC: Adenylyl cyclase 6 improves calcium uptake and left ventricular function in aged hearts. J Am Coll Cardiol 57: 1846-1855, 2011.
54. Han F, Hou N, Liu Y, Huang N, Pan R, Zhang X, Mao E and Sun X: Liraglutide improves vascular dysfunction by regulating a cAMP-independent PKA-AMPK pathway in perivascular adipose tissue in obese mice. Biomed Pharmacother 120: 109537, 2019.